光学学报

基于自由曲面的紧凑型宽波段成像光谱仪设计

韩继周[1,2,3]，赵世家[1,2,3]，冯安伟[1,2,3]，张幸运[1,2,3]，季轶群[1,2,3*]

[1]苏州大学光电科学与工程学院，江苏 苏州 215006；
[2]江苏省先进光学制造技术重点实验室 & 教育部现代光学技术重点实验室，江苏 苏州 215006；
[3]苏州纳米科技协同创新中心 & 数码激光成像与显示教育部工程研究中心，江苏 苏州 215006

摘要 针对基于传统光学元件的成像光谱仪，在实现大视场与宽波段的同时难以满足结构紧凑的问题，在Offner成像光谱仪的第三反射镜引入圆锥曲面叠加条纹泽尼克多项式表征的自由曲面。基于矢量像差理论，分析了四阶以下的泽尼克多项式在系统中引入的像散与系统视场、波长的关系，通过选取合理的多项式叠加到圆锥曲面，设计了一款工作于可见光到短波红外波段（400～2500 nm）、体积仅42 mm×82 mm×100 mm的成像光谱仪。系统实现了双波段探测，来自两个不同宽度狭缝的光线经光栅分光后，通过分束器将工作波段分为可见近红外（400～1000 nm）和短波红外（1000～2500 nm），优化设计结果表明，光谱分辨率分别为2.8 nm和4 nm，成像质量良好，为实现宽波段紧凑型成像光谱仪的设计提供了理论参考。

关键词 光学设计；自由曲面；成像光谱仪；Offner结构；宽波段

中图分类号 TH74 **文献标志码** A **DOI：** 10.3788/AOS230474

1 引言

成像光谱仪可以同时获取目标物体的空间信息和光谱信息[1]，其在地物分析、空间遥感、目标侦察等方面有着广泛的应用前景[2-7]。随着光谱技术的发展，设计者希望成像光谱仪在满足小体积的同时可以实现更大的视场与更宽的波段，Offner成像光谱仪在这方面表现出优异的能力。但随着视场与波段的增大，校正像差的困难程度也在加大，采用传统光学元件的Offner成像光谱仪，往往通过放宽尺寸的限制或在光路增加校正透镜来平衡像差，因此会引起系统体积或质量的增大，无法满足系统轻小型化的要求。

随着加工与检测技术的不断发展[8-9]，自由曲面逐渐被广泛地应用到光学设计中[10-11]。自由曲面是一种非旋转对称的光学元件，可以在光学设计中引入更多的自由度，进而提升像差的校正能力。近年来，已不断有研究者将自由曲面应用到成像光谱仪中。2017年，Reimers等[12]在Chrisp-Offner型成像光谱仪中将主镜、光栅与第三反射镜均设计为自由曲面，设计了一款波段为200～1500 nm的成像光谱仪系统，与使用全球面的系统相比，体积是其1/5，说明了自由曲面在减小成像光谱仪体积方面有着巨大潜力。2018年，Yang等[13]将“点对点”的设计方法应用于自由曲面成像光谱仪中，实现了自由曲面光谱仪的自动化设计，并设计了一款体积仅为41 cm^3的离轴三反型成像光谱仪，其波段为450～950 nm，其两片反射镜与反射光栅均引入了自由曲面。同年，Feng等[14]设计了一种双波段的自由曲面Offner曲面棱镜成像光谱仪，实现了400～2500 nm的超宽波段光谱成像，但体积为280 mm×180 mm×100 mm，不够紧凑，且色散线性度较差。2021年，Zhang等[15]使用矢量像差理论去分析Offner光栅成像光谱仪，最终设计了一款体积约为305 cm^3的成像光谱仪，工作波段为400～1000 nm，但其自由曲面采用了7阶xy多项式表征，较为复杂且冗长。

在成像光谱仪中引入自由曲面可以提升系统的像差校正能力，但光学系统使用过多自由曲面或光学表面引入过多的自由曲面项，会引起表面矢高的大幅度偏离，这不仅会降低系统中自由曲面的像差校正能力，还会增大自由曲面制造和检测的难度[16-17]，因此，在成像光谱仪设计中使用合理的自由曲面颇为关键。本文针对采用圆锥曲面叠加条纹泽尼克多项式表征的自由曲面，基于矢量像差理论计算并分析了各多项式在系统中引入像散与视场及波长这两者的关系，最终通过

收稿日期：2023-01-13；**修回日期**：2023-02-14；**录用日期**：2023-03-20；**网络首发日期**：2023-05-05

基金项目：国家自然科学基金（61405134，61340007）、国防基础科研计划（JCKY2018414C013）、江苏省自然科学基金（BK20161512）、江苏高校优势学科建设工程资助项目（PAPD）

通信作者：*jiyiqun@suda.edu.cn

选取合理的多项式进行优化，设计了一款工作波段为400～2500 nm 的宽波段成像光谱仪，体积仅为42 mm×82 mm×100 mm，其中仅第三反射镜设计为自由曲面且面型表达式中只使用了3项自由曲面项。该系统实现了可见近红外（400～1000 nm）和短波红外（1000～2500 nm）的双波段探测，优化设计结果表明，光谱分辨率分别为2.8 nm和4 nm，全视场全波段在奈奎斯特频率处的调制传递函数（MTF）值均大于0.5，谱线弯曲与色畸变均小于10%像元大小，成像质量良好，为实现宽波段紧凑型成像光谱仪的设计提供了理论参考。

2 设计思想

2.1 Offner成像光谱仪中的三阶像散

Offner成像光谱仪的光路示意图如图1所示，其中M_1与M_3为凹面反射镜，M_2为凸面光栅，3个元件拥有共同的球心。根据矢量像差理论[18]，计算得到Offner成像光谱仪中3阶像差的表达式为

$$\begin{aligned}W(\overrightarrow{H^\#},\vec{\rho})=&W_{040}(\vec{\rho}\cdot\vec{\rho})^2+W_{131}[(\overrightarrow{H^\#}-\overrightarrow{\sigma_j})\cdot\vec{\rho}](\vec{\rho}\cdot\vec{\rho})+W_{220M}[(\overrightarrow{H^\#}-\overrightarrow{\sigma_j})\cdot(\overrightarrow{H^\#}-\overrightarrow{\sigma_j})](\vec{\rho}\cdot\vec{\rho})+\\&\frac{1}{2}W_{222}[(\overrightarrow{H^\#}-\overrightarrow{\sigma_j})^2\cdot\vec{\rho}^2]+W_{311}[(\overrightarrow{H^\#}-\overrightarrow{\sigma_j})\cdot(\overrightarrow{H^\#}-\overrightarrow{\sigma_j})][(\overrightarrow{H^\#}-\overrightarrow{\sigma_j})\cdot\vec{\rho}],\end{aligned}\tag{1}$$

$$\overrightarrow{H^\#}=\vec{H}+\vec{h},\tag{2}$$

式中：$\vec{H}$和$\vec{\rho}$分别为归一化的视场矢量与光瞳矢量；$\vec{h}$为视场偏心矢量，用于表示光瞳离轴的系统中视场在另一维度上的偏移，如图1所示，在Offner成像光谱仪中即为垂直于狭缝方向上的视场偏移；$\overrightarrow{H^\#}$为等效视场偏心矢量；$\overrightarrow{\sigma_j}$为像差场偏心矢量，它是由色散引起像差场在光谱方向的偏心矢量；W_{040}、W_{131}、W_{220M}、W_{222}、W_{311}分别表示球差、彗差、场曲、像散、畸变5种波前像差系数。

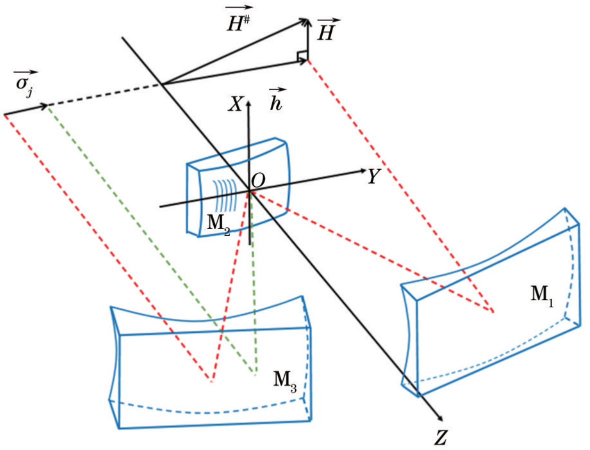

图1 Offner成像光谱仪光路示意图

Fig. 1 Schematic diagram of optical path of Offner imaging spectrometer

Offner成像光谱仪中的主要像差为像散，由式（1）中的第4项和式（2），可以得到Offner成像光谱仪中的3阶像散表达式为

$$\begin{aligned}W_{\mathrm{asti}}=&\frac{1}{2}[W_{222}(\vec{H}+\vec{h})^2-2(\vec{H}+\vec{h})(W_{222}\overrightarrow{\sigma_j})+\\&W_{222}\overrightarrow{\sigma_j}^2]\cdot\vec{\rho}^2。\end{aligned}\tag{3}$$

由于$\vec{H}$和$\overrightarrow{\sigma_j}$的方向始终相互垂直，$\vec{h}$和$\overrightarrow{\sigma_j}$的方向始终平行，由式（3）可以得出，Offner成像光谱仪中像散会随着视场和波长的增大而增大，在大视场与宽波段的设计要求下，传统元件的像差校正能力有限，无法获得良好的像质。

2.2 Offner中使用自由曲面引入的三阶像散

在Offner成像光谱仪中，将M_3镜引入自由曲面可以同时校正与视场和色散相关的像差，为最佳选择[15]。以二次曲面为基底叠加泽尼克多项式的自由曲面矢高表达式为

$$z=\frac{c(x^2+y^2)}{1+\sqrt{1-(1+k)c^2(x^2+y^2)}}+\sum_{j=1}^{n}C_jZ_j,\tag{4}$$

式中：c表示表面的曲率；k表示conic系数；Z_j表示第j项泽尼克多项式；C_j表示其对应的系数。泽尼克多项式是一种φ多项式[19]，除了传统的笛卡儿坐标表达式，也可以用极坐标表示为

$$Z_j=F(\rho,\phi),\tag{5}$$

式中：ρ表示归一化半径；ϕ表示幅角。根据多项式排序的不同，泽尼克多项式又分为标准泽尼克多项式和条纹泽尼克多项式，本文中均使用条纹泽尼克多项式，其中第1到18项的表达式如表1所示。

因为Offner成像光谱仪不存在中间像面[20]，则系统中各泽尼克多项式引入的像差表达式为

$$W_j=-\frac{2}{\lambda}\overrightarrow{C_j}\cdot Z_j(\vec{\rho})=-\frac{2}{\lambda}\overrightarrow{C_j}\cdot Z_j(\overrightarrow{\rho_x},\overrightarrow{\rho_y}),\tag{6}$$

式中：λ表示波长；j表示对应的项数，当使用的是成对的泽尼克项时，如Z_5和Z_6、Z_7和Z_8，$Z(\vec{\rho})=Z(\rho,\phi)=\begin{bmatrix}Z_x(\rho,\phi)\\Z_y(\rho,\phi)\end{bmatrix}$，$\vec{C}=C\mathrm{e}^{\mathrm{i}\alpha}$是其对应的系数矢量，它的大小$C=\sqrt{C_x^2+C_y^2}$，方向$\alpha=\arctan(C_y/C_x)$，当使用的是单独的泽尼克项时，如$Z_9$、$Z_{16}$，$\vec{C}\cdot Z(\vec{\rho})=CZ(\rho)$。

在Offner成像光谱仪中，由于是将光栅设置为光阑，M_3镜是一远离光阑的表面，除零视场外其他视场的光瞳使用的是M_3镜的偏心区域，如图2（a）所示，引入$\Delta\overrightarrow{h_H}$用来表示光瞳随着视场的偏移，此时自由曲面

表1 条纹泽尼克多项式

Table 1 Fringe Zernike polynomial

Term	Zernike polynomial	Term	Zernike polynomial	Term	Zernike polynomial
Z_1	1	Z_7	$(3\rho^3-2\rho)\cos\phi$	Z_{13}	$(4\rho^4-3\rho^2)\sin(2\phi)$
Z_2	$\rho\cos\phi$	Z_8	$(3\rho^3-2\rho)\sin\phi$	Z_{14}	$(10\rho^5-12\rho^3+3\rho)\cos\phi$
Z_3	$\rho\sin\phi$	Z_9	$6\rho^4-6\rho^2+1$	Z_{15}	$(10\rho^5-12\rho^3+3\rho)\sin\phi$
Z_4	$2\rho^2-1$	Z_{10}	$\rho^3\cos(3\phi)$	Z_{16}	$20\rho^6-30\rho^4+12\rho^2-1$
Z_5	$\rho^2\cos(2\phi)$	Z_{11}	$\rho^3\sin(3\phi)$	Z_{17}	$\rho^4\cos(4\phi)$
Z_6	$\rho^2\sin(2\phi)$	Z_{12}	$(4\rho^4-3\rho^2)\cos(2\phi)$	Z_{18}	$\rho^4\sin(4\phi)$

实际使用的光瞳矢量则为

$$\vec{\rho}'=\vec{\rho}+\Delta\vec{h}_H。\tag{7}$$

由于光线经过光栅之后会发生色散，在经过M_3镜时，不同波长的光瞳使用的也是其偏心区域，如图2(b)所示，引入$\Delta\vec{h}_\lambda$来表示光瞳由于色散而引起的偏移，此时自由曲面实际使用的光瞳矢量则为

$$\vec{\rho}''=\vec{\rho}+\Delta\vec{h}_\lambda。\tag{8}$$

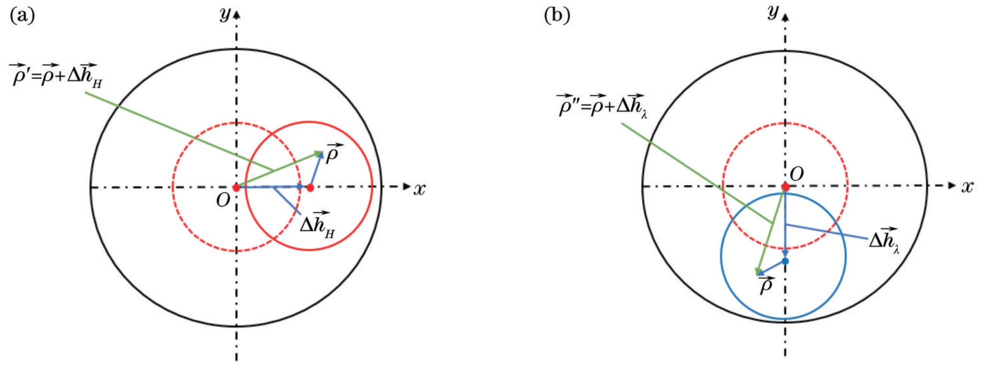

图2 光瞳偏移示意图。(a)轴外视场光瞳偏移示意图；(b)色散光瞳偏移示意图

Fig. 2 Schematic diagram of pupil shift . (a) Schematic diagram of pupil shift in off-axis field; (b) schematic diagram of pupil shift for dispersion

在Offner成像光谱仪中，M_1镜和M_3镜的倾斜角度一般较小，在此不考虑由于元件倾斜引起的光瞳的缩放，将其看作是圆形光瞳。狭缝方向为x方向，则色散方向为y方向，将式(7)和式(8)代入式(6)，并用M表示其系数$-2C/\lambda$，可以得到M_3镜由泽尼克多项式引入的像差表达式为

$$W=\sum_{j=1}^{n}M_j\cdot Z_j(\rho_x+\Delta h_{Hx},\rho_y+\Delta h_{\lambda y})。\tag{9}$$

由式(9)展开，可以计算得出M_3镜设计为自由曲面时，不同泽尼克项引入的泽尼克像散表达式，由于系统是关于yOz平面对称的，使用时仅考虑关于yOz平面对称的自由曲面项，且使用时通常仅使用4阶及以下的泽尼克项，总结如表2所示。

由表2计算的表达式可以得出各项引入的像散与系统的波长和视场的关系，其中，Z_5项引入的像散值是常数，与视场或波长无关；Z_8与Z_{11}项引入的像散中，Z_5分量的系数是与$\Delta h_{\lambda y}$线性相关的，而Z_6分量的系数是与Δh_{Hx}线性相关的，表明Z_8与Z_{11}项引入的像散是可以同时随着视场和波长的增大而增大的；Z_9与Z_{17}项引入的像散中，如图3(a)和3(b)所示，Z_6分量的系数可以看作是与视场或波长线性相关的，如图3(c)和3(d)所示，Z_5分量的系数是与视场或波长非线性相关的，所以Z_9与Z_{17}项引入的像散不会同时随着视场和波长的增大而增大；Z_{12}引入的像散虽然与视场或波长是非线性相关的，但其值是可以同时随着视场和波长的增大而增大的。由2.1节的分析可以得知，Offner成像光谱仪中像散会随着视场和波长的增大而增大，所以当自由曲面引入的像散可以同时随着视场和波长的增大而增大时，是有利于像散的校正的。结合上述分析可得，在Offner光栅成像光谱仪中引入自由曲面实现大视场和宽波段的优化设计中，当选用4阶及以下的泽尼克自由曲面项时，选择Z_8、Z_{11}、Z_{12}可以对整个大视场

表2　不同泽尼克项引入的像散

Table 2　Astigmatism generated by different Zernike terms

Zernike term added on surface	Generated Zernike astigmatism	
	Z_5	Z_6
M_5Z_5	M_5Z_5	—
M_8Z_8	$-3\Delta h_{\lambda y}M_8Z_5$	$3\Delta h_{Hx}M_8Z_6$
M_9Z_9	$(12\Delta h_{Hx}^2-12\Delta h_{\lambda y}^2)M_9Z_5$	$24\Delta h_{Hx}\Delta h_{\lambda y}M_9Z_6$
$M_{11}Z_{11}$	$3\Delta h_{\lambda y}M_{11}Z_5$	$3\Delta h_{Hx}M_{11}Z_6$
$M_{12}Z_{12}$	$(12\Delta h_{Hx}^2+12\Delta h_{\lambda y}^2)M_{12}Z_5$	—
$M_{17}Z_{17}$	$(6\Delta h_{Hx}^2-6\Delta h_{\lambda y}^2)M_{17}Z_5$	$-12\Delta h_{Hx}\Delta h_{\lambda y}M_{17}Z_6$

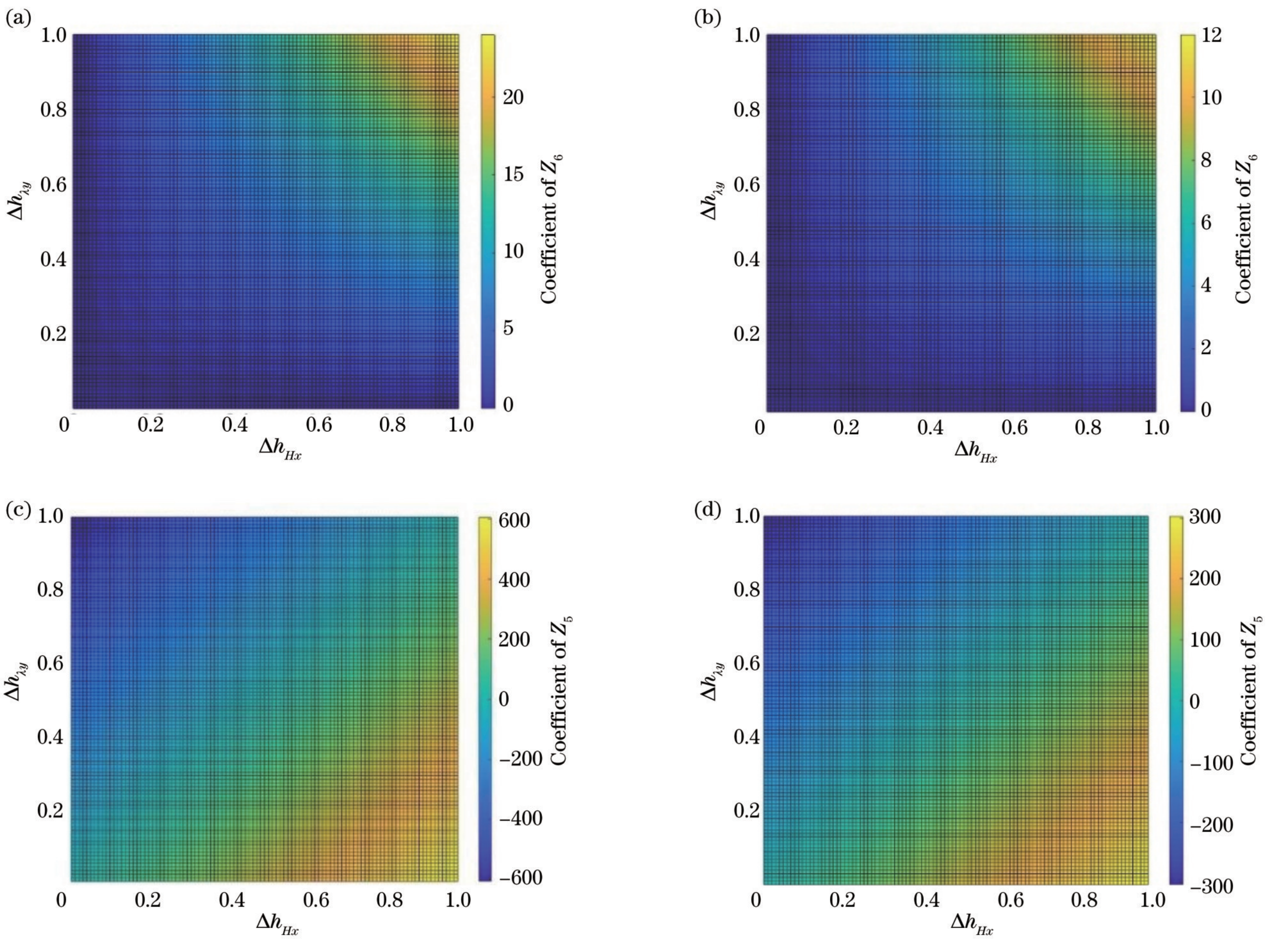

图3　泽尼克项引入的像散系数表达式函数图。(a) Z_9项引入的Z_6系数表达式函数图；(b) Z_{17}项引入的Z_6系数表达式函数图；(c) Z_9项引入的Z_5系数表达式函数图；(d) Z_{17}项引入的Z_5系数表达式函数图

Fig. 3　Diagram of expression function of astigmatism coefficient introduced by Zernike terms. (a) Functional diagram of coefficient expressions introduced into Z_6 by Z_9 term; (b) functional diagram of coefficient expressions introduced into Z_6 by Z_{17} term; (c) functional diagram of coefficient expressions introduced into Z_5 by Z_9 term; (d) functional diagram of coefficient expressions introduced into Z_5 by Z_{17} term

与宽波段范围内的像散进行校正。

3　设计结果与像质评价

3.1　系统设计

为验证第2.2节分析得到的结论，设计了一款宽波段的成像光谱仪，其结构示意图如图4所示，其中光栅的刻线密度为100 lp/mm，并选用−1级衍射级次，其波段覆盖400～2500 nm，系统设计为可见近红外(VNIR)和短波红外(SWIR)双波段探测，采用宽度不同的两个狭缝以保证每个波段独立的光谱分辨率，来

自双狭缝的光线依次经过M_1、M_2和M_3后，通过一个半透半反的滤光片作为分束器将两个波段分别成像于对应的探测器，其中VNIR波段使用的探测器像元大小为14 μm，SWIR波段使用的探测器像元大小为20 μm，系统的指标参数如表3所示，其中M_3镜设计为自由曲面。在最终优化设计之前，使自由曲面仅选择单个泽尼克项，分别对系统进行优化后，得到在边缘视场及2500 nm波长时泽尼克像散大小如图5所示，可以看出，选择Z_5、Z_9、Z_{17}进行优化时系统的像散并没有得到校正，而选择Z_8、Z_{11}、Z_{12}时有效减小了系统的像散，验证了2.2节得出的结论，最终同时选择Z_8、Z_{11}、Z_{12}项进行优化设计，得到的系统基本参数如表4所示，M_3镜使用的泽尼克项系数如表5所示。

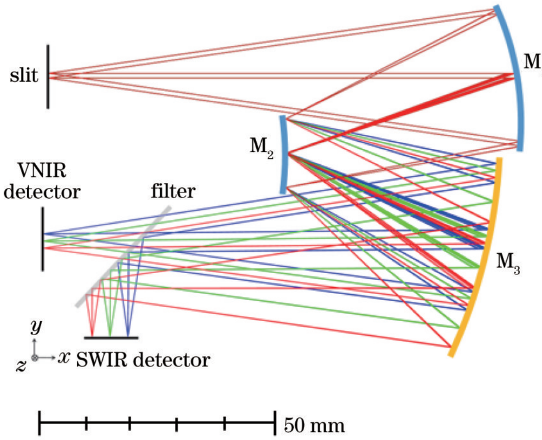

图4 双波段Offner成像光谱仪结构示意图

Fig. 4 Structure diagram of dual-band Offner imaging spectrometer

表3 Offner成像光谱仪的指标参数

Table 3 Specifications of Offner imaging spectrometer

Parameter	Value	Unit
Wavelength for VNIR	400-1000	nm
Wavelength for SWIR	1000-2500	nm
Numerical aperture	0.143	
Length of slit	14	mm
Spectral channel	≥589	
Spectral resolution	2.8/4	nm
Volume	42×82×100	mm^3

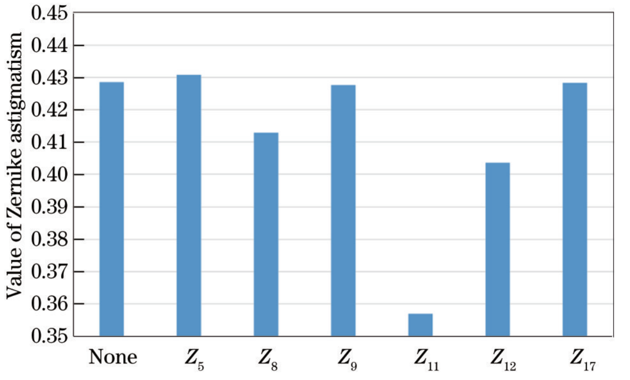

图5 M_3镜分别选择单个不同泽尼克项设计时系统的泽尼克像散

Fig. 5 Zernike astigmatism of system when designing with individual different Zernike terms for M_3 mirror

表4 系统的基本参数

Table 4 Basic parameters of system

Element	Curvature radius /mm	Distance /mm	Tilt angle /(°)
Entrance slit	—	98.67	0
M_1	−101.62	−51.83	−8.59
M_2 (diffraction grating)	−51.41	42.93	0
M_3	−95.37	−72.94	13.14
Filter	—	−18.81	45
Image plane	—	—	0

表5 M_3镜使用的泽尼克项系数

Table 5 Coefficient of Zernike terms in M_3

Term	Z_8	Z_{11}	Z_{12}
Coefficient	5.3287×10^{-4}	-2.8874×10^{-4}	4.5452×10^{-5}

3.2 像质评价

在M_3镜设计为自由曲面进行优化的同时，也对M_3镜设计为球面且保持体积不变以及M_3镜设计为球面且体积放大到60 mm×110 mm×150 mm的情况进行优化，如图6所示，给出了在视场分别为0、4、7 mm时，三种情况下全波段像点的均方根（RMS）半径大小曲线图，黑色的直线表示爱里斑的RMS半径。如图6(a)所示，M_3设计为自由曲面时全视场全波段处RMS半径均小于6 μm，小于单个像元大小，像质良好；如图6(b)所示，M_3设计为球面且体积保持不变时全视场全波段处RMS半径都有明显增大，像质明显下降；如图6(c)所示，M_3设计为球面但体积放大了约3倍时，全视场全波段处RMS半径与图6(a)所示情况接近，像质良好。可以看出，M_3设计为自由曲面在保持了良好像质的同时，有效地缩小了系统的体积。

如图7所示，给出了M_3镜设计为自由曲面时系统在400、1450、2500 nm处的MTF曲线，在其对应的奈奎斯特频率处MTF值均大于0.5。

如图8所示，给出了系统的谱线弯曲与色畸变，其最大谱线弯曲与色畸变在两个波段处均小于10%像元大小。

4 结　论

基于传统光学元件的成像光谱仪在实现大视场与宽波段时，往往通过放宽尺寸的限制或在光路增加校正透镜来平衡像差，使得结构不够紧凑。引入自由曲面可以使系统在小型化的前提下提升像差校正能力，

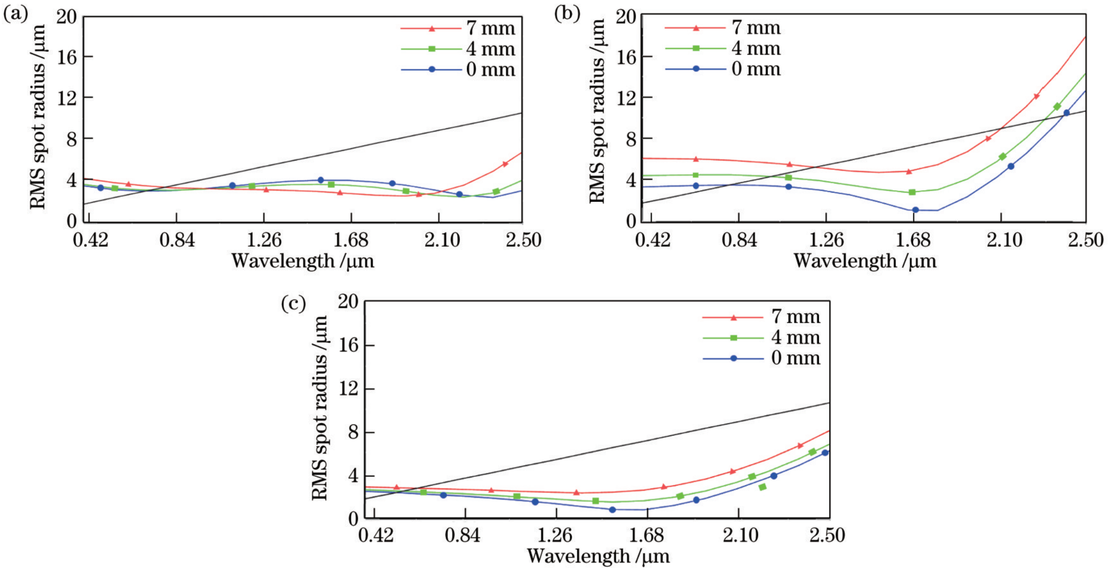

图 6　成像光谱仪全波段像点RMS半径。(a) M_3镜设计为自由曲面；(b) M_3镜设计为球面；(c) M_3镜设计为球面且体积放大约3倍

Fig. 6　Image point RMS radii for full wavelength bands of imaging spectrometer. (a) M_3 is designed as a free-form surface; (b) M_3 is designed as a spherical surface; (c) M_3 is designed as a spherical surface and system size is enlarged by approximately three times

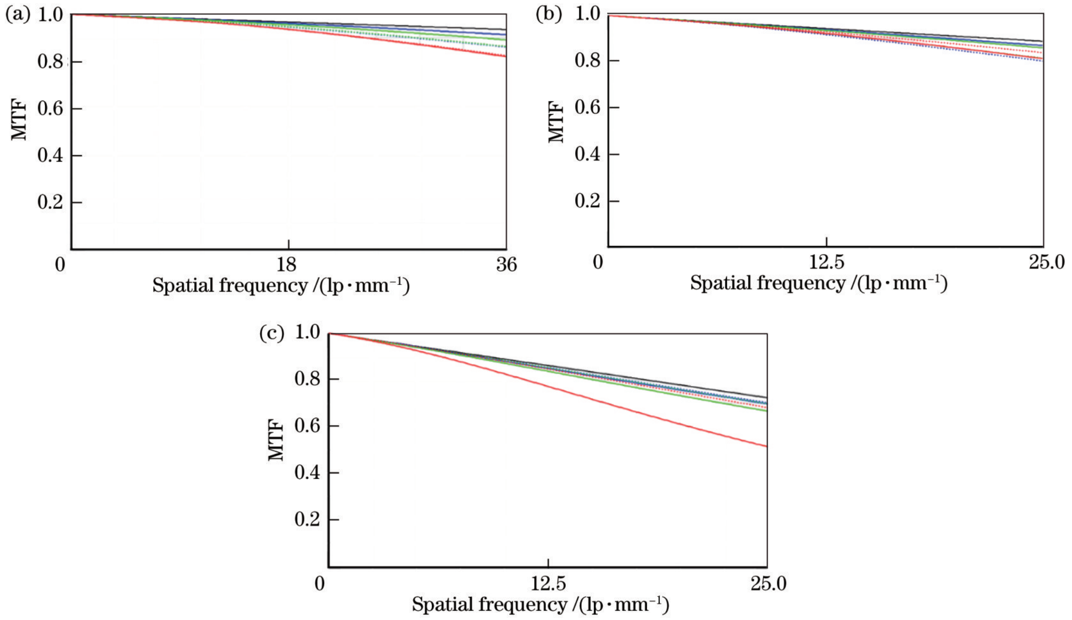

图 7　成像光谱仪不同波长处的MTF。(a) 400 nm；(b) 1450 nm；(c) 2500 nm

Fig. 7　MTF at different wavelengths of imaging spectrometer. (a) 400 nm; (b) 1450 nm; (c) 2500 nm

但是系统中使用过多的自由曲面或自由曲面的表达式中使用过多的多项式，都有可能造成自由曲面像差校正能力的降低和制造难度的增大，因此设计时合理使用自由曲面颇为关键。本文基于矢量像差理论，分析了4阶以下的条纹泽尼克多项式在Offner成像光谱仪中引入的像散与系统视场、波长的关系，其中第8、第11和第12项引入的像散会随视场和波长的增大而增大，设计时选取这3项可以对整个大视场与宽波段范围内的像散进行校正。最终设计了一款成像光谱仪，其工作波段覆盖可见光到短波红外(400～2500 nm)，体积仅为42 mm×82 mm×100 mm，同时实现了宽波段与紧凑结构。其中仅第三反射镜设计为自由曲面，其面型表达式采用圆锥曲面叠加第8、第11和第12项条纹泽尼克多项式表征。系统实现了可见近红外(400～1000 nm)和短波红外(1000～2500 nm)双波段探测，来自两个不同宽度狭缝的光线经光栅分光后，通过分束器将工作波段分为两部分，分别成像于可见近红外探测器和短波红外探测器，优化设计结果表明，光谱分辨率分别为2.8 nm和4 nm，谱线弯曲与色畸变均小于10%像元，全视场全波段在奈奎斯特频率处的MTF值均大于0.5，成像质量良好，为实现宽波段紧凑型成像光谱仪的设计提供了理论参考。

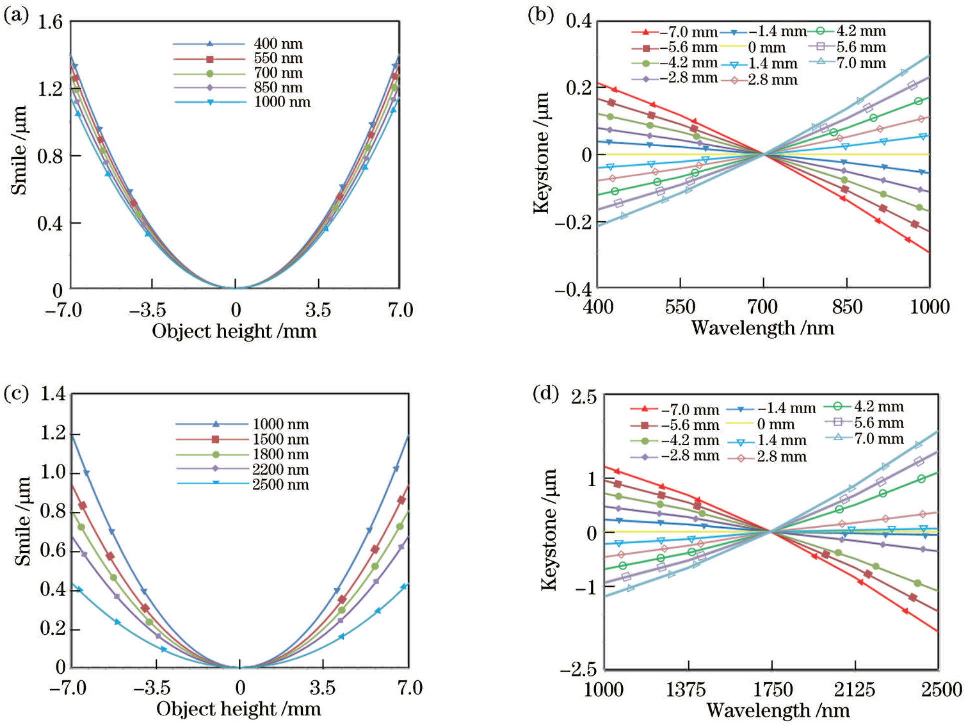

图 8 成像光谱仪两个波段的谱线弯曲和色畸变。(a) VNIR 波段谱线弯曲；(b) VNIR 波段色畸变；(c) SWIR 波段谱线弯曲；(d) SWIR 波段色畸变

Fig. 8 Smiles and keystones in two bands of imaging spectrometer. (a) Smiles for VNIR; (b) keystones for VNIR; (c) smiles for SWIR; (d) keystones for SWIR

参 考 文 献

[1] Hagen N A, Kudenov M W. Review of snapshot spectral imaging technologies[J]. Optical Engineering, 2013, 52(9): 090901.

[2] Chrisp M P, Lockwood R B, Smith M A, et al. Development of a compact imaging spectrometer form for the solar reflective spectral region[J]. Applied Optics, 2020, 59(32): 10007-10017.

[3] 于磊, 陈结祥, 薛辉, 等. 用于沿海水色探测的机载紫外-可见-近红外高光谱成像仪[J]. 光学 精密工程, 2018, 26(10): 2363-2370.
Yu L, Chen J X, Xue H, et al. Hyper-spectral imaging sensor in UV-VIS-NIR region in air for coastal ocean observation[J]. Optics and Precision Engineering, 2018, 26(10): 2363-2370.

[4] 罗刚银, 王弼陡, 陈玉琦, 等. 可见近红外波段无人机载成像光谱仪设计[J]. 光子学报, 2017, 46(9): 0930001.
Luo G Y, Wang B D, Chen Y Q, et al. Design of visible near infrared imaging spectrometer on unmanned aerial vehicle[J]. Acta Photonica Sinica, 2017, 46(9): 0930001.

[5] 朱嘉诚, 陆伟奇, 赵知诚, 等. 静止轨道中波红外成像光谱仪分光成像系统[J]. 光学学报, 2021, 41(11): 1122001.
Zhu J C, Lu W Q, Zhao Z C, et al. Spectroscopic imaging system in mid-wave infrared imaging spectrometer on geostationary orbit[J]. Acta Optica Sinica, 2021, 41(11): 1122001.

[6] Feng A W, Zhao S J, Han J Z, et al. High spectral resolution compact Offner spectrometer based on the aberration-reduced convex holographic gratings recorded by spherical waves under Rowland circle mounting[J]. Applied Optics, 2022, 61(13): 3893-3900.

[7] 谭奋利, 曾晨欣, 冯安伟, 等. 基于Dyson结构的新型快照式分光成像系统光学设计[J]. 光学学报, 2022, 42(4): 0422002.
Tan F L, Zeng C X, Feng A W, et al. Optical design of novel snapshot spectral imaging system based on Dyson structure[J]. Acta Optica Sinica, 2022, 42(4): 0422002.

[8] Benjamin R J, Saito T T. Diamond turning at a large optical manufacturer[J]. International Society for Optics and Photonics, 1978, 17: 81-87.

[9] Stuerwald S. Error compensation in computer generated hologram-based form testing of aspheres[J]. Applied Optics, 2014, 53(35): 8249-8255.

[10] 杨晓彤, 张国玉, 张健, 等. 用于太阳直接辐射测量的自由曲面反射镜优化设计方法[J]. 光学学报, 2022, 42(9): 0922001.
Yang X T, Zhang G Y, Zhang J, et al. Optimization design method of freeform reflector for direct solar radiation measurement[J]. Acta Optica Sinica, 2022, 42(9): 0922001.

[11] 周彦辰, 郭亮, 陈志涛, 等. 基于全内反射结构的多自由曲面准直透镜设计[J]. 光学学报, 2021, 41(4): 0422003.
Zhou Y C, Guo L, Chen Z T, et al. Design of collimating lens with multiple freeform surfaces based on total internal reflection structure[J]. Acta Optica Sinica, 2021, 41(4): 0922003.

[12] Reimers J, Thompson K P, Troutman J, et al. Increased compactness of an imaging spectrometer enabled by freeform surfaces[C]//Optical Design and Fabrication 2017 (Freeform, IODC, OFT), July 9-13, 2017, Denver, Colorado. Washington, D.C.: Optica Publishing Group, 2017: JW2C.

[13] Yang T, Cheng D W, Wang Y T. Freeform imaging spectrometer design using a point-by-point design method[J]. Applied Optics, 2018, 57(16): 4718-4727.

[14] Feng L, Zhou J S, Wei L D, et al. Design of a compact wide-spectrum double-channel prism imaging spectrometer with freeform surface[J]. Applied Optics, 2018, 57(31): 9512-9522.

[15] Zhang J L, Zheng Y Q, Lin C, et al. Analysis method of the Offner hyperspectral imaging spectrometer based on vector aberration theory[J]. Applied Optics, 2021, 60(2): 264-275.

[16] Fuerschbach K, Thompson K P, Rolland J P. Interferometric measurement of a concave, φ-polynomial, Zernike mirror[J]. Optics Letters, 2014, 39(1): 18-21.

[17] Forbes G W. Manufacturability estimates for optical aspheres[J]. Optics Express, 2011, 19(10): 9923-9941.

[18] Thompson K. Description of the third-order optical aberrations of near-circular pupil optical systems without symmetry[J]. Journal of the Optical Society of America A, 2005, 22(7): 1389-1401.

[19] Fuerschbach K, Rolland J P, Thompson K P. A new family of optical systems employing φ-polynomial surfaces[J]. Optics Express, 2011, 19(22): 21919-21928.

[20] Yang T, Cheng D W, Wang Y T. Aberration analysis for freeform surface terms overlay on general decentered and tilted optical surfaces[J]. Optics Express, 2018, 26(6): 7751-7770.

Design of Compact and Broadband Imaging Spectrometer Based on Free-Form Surface

Han Jizhou[1,2,3], Zhao Shijia[1,2,3], Feng Anwei[1,2,3], Zhang Xingyun[1,2,3], Ji Yiqun[1,2,3*]

[1] *School of Optoelectronic Science and Engineering, Soochow University, Suzhou* 215006, *Jiangsu, China*;

[2] *Key Lab of Advanced Optical Manufacturing Technologies of Jiangsu Province & Key Lab of Modern Optical Technologies of Education Ministry of China, Suzhou* 215006, *Jiangsu, China*;

[3] *Collaborarive Innovation Center of Suzhou Nano Science and Technology & Engineering Research Center of Digital Imaging and Display, Ministry of Education, Suzhou* 215006, *Jiangsu, China*

Abstract

Objective Imaging spectrometer can obtain spatial and spectral information of targets simultaneously, and it has been widely applied in ground object analysis, space remote sensing, target reconnaissance, and other aspects. As spectral imaging technology develops, designers hope that the imaging spectrometer can achieve a wider field of view (FOV) and wavelength band while meeting the structural compactness. In this aspect, the Offner imaging spectrometer shows excellent performance. However, with the expanding FOV and wavelength band, the aberration correction is more difficult. The Offner imaging spectrometer employing a traditional spherical mirror usually balances aberration by relaxing the size limits or adding lenses to the system, thereby leading to the increasing volume or complexity but failing to meet the requirements of lightweight and compactness. With the development of manufacturing and testing technology, the free-form surface has been widely employed in optical design. It is a kind of non-rotationally symmetric optical element, which can introduce more degrees of freedom into optical design. Introducing free-form surfaces into imaging spectrometers can improve the aberration correction ability of the system. However, too many free-form surfaces in optical systems or too many free-form terms on optical surfaces will cause a large deviation in the sag of surfaces, which will not only reduce the aberration correction ability of free-form surfaces in the system but also make the manufacturing of free-form surfaces more difficult. Therefore, we want to use a reasonable free-form surface in the imaging spectrometer design to achieve broad wavelength band and compact volume simultaneously.

Methods The main aberration in the Offner imaging spectrometer is astigmatism. Firstly, the expression of the third-order astigmatism of the system is obtained based on the vector aberration theory. The analysis of the expression of third-order astigmatism shows that the astigmatism of the system increases with the increase of FOV and wavelength band. In the Offner imaging spectrometer, the design of the third mirror as a free-form surface allows for the correction of aberrations associated with both FOV and dispersion. Then we calculate the expression for astigmatism introduced in the Offner imaging spectrometer by Zernike polynomials of 4th order and below when the third mirror is designed as a free-form surface with conical surface adding fringe Zernike polynomials. In the calculation, since the diffraction grating is set as aperture stop and the third mirror is a surface away from the stop, the pupil employed in the non-central FOV is shifted relative to the central FOV, and an offset vector is introduced to describe the pupil utilized by the non-center field on the third mirror. Additionally, since the third mirror is set behind the grating in the system, the rays passing through the grating have been dispersed on the third mirror, and the other offset vector is introduced to describe the pupil region leveraged by the rays with different wavelengths on the third mirror at this time. Finally, the relationship among the introduced astigmatism, wavelength, and FOV of the system can be obtained by analyzing the calculated expressions. The results show that in the optical design of the Offner imaging spectrometer based on free-form surfaces when Zernike free-form terms of 4th order and below are selected, the eighth, eleventh, and twelfth terms of Zernike polynomial can be selected to correct astigmatism in the wide FOV and wavelength band.

Results and Discussions An imaging spectrometer with broad wavelength band is designed, and its structure is shown in

Fig. 4. The groove density of grating is 100 lp/mm and the diffraction order of −1 is selected, with a wavelength band from 400 to 2500 nm. The system is designed for dual-band detection of visible-near-infrared (VNIR) and shortwave-infrared (SWIR). Two slits with different widths are adopted to ensure the independent spectral resolution of each band. After the rays from the dual slit pass through M_1, M_2, and M_3 successively, they are imaged to corresponding detectors respectively through a dichroic mirror as a beam splitter. The detectors have pixels of 14 μm for the VNIR band and 20 μm for the SWIR band. The system specifications are shown in Table 3 and the lens data of the system are shown in Table 4. M_3 is designed as a free-form surface. The coefficients of different Zernike terms in M_3 are shown in Table 5. The volume of the system is 42 mm×82 mm×100 mm, which is one-third of the spherical mirror system with the same specifications.

Conclusions The imaging spectrometer based on the conventional optical element is difficult to meet the structural compactness and realize wide FOV and wavelength. Thus, the third mirror in the Offner imaging spectrometer is designed as a free-form surface expressed by a conical surface with fringe Zernike polynomial added. The relations among astigmatism introduced by polynomials of fourth order and below, wavelength, and FOV in the Offner imaging spectrometer based on vector aberration theory are analyzed. Then an imaging spectrometer with a wavelength range from 400 to 2500 nm and a volume of only 42 mm×82 mm×100 mm is proposed by selecting a reasonable polynomial adding on a conical surface. The system achieves dual-band detection. The rays from two slits with different widths are dispersed by the diffraction grating from the beam splitter to work in visible-near-infrared (400–1000 nm) and shortwave-infrared (1000–2500 nm) bands. The optimized design results indicate that the spectral resolution is 2.8 nm and 4 nm respectively with high imaging quality. Finally, theoretical reference implications are provided for the application of free-form surfaces in the design of imaging spectrometers.

Key words optical design; free-form surface; imaging spectrometer; Offner structure; broadband